# NEW EXPERIMENTAL MEASUREMENTS OF ELECTRON CLOUDS IN ION BEAMS WITH LARGE TUNE DEPRESSION*

A.W.Molvik**, M. Kireeff Covo, A. Friedman, R. Cohen, S.M. Lund, W. Sharp, LLNL, Livermore, CA 94550, U.S.A.
F. Bieniosek, C. M. Leister, P. Seidl, D. Baca, J-L. Vay, LBNL, Berkeley, CA 94720-8201, U.S.A.

*Abstract*

We study electron clouds in high perveance beams (K = 8E-4) with a large tune depression of 0.10 (defined as the ratio of a single particle oscillation response to the applied focusing fields, with and without space charge). These 1 MeV, 180 mA, K+ beams have a beam potential of +2 kV when electron clouds are minimized. Simulation results are discussed in companion papers.

We have developed new quantitative measurements, including the first quantitative measurements of the accumulation of electrons in a positively-charged beam. This, together with measurements of electron sources, will enable the electron particle balance to be measured, and electron-trapping efficiencies determined. We also measure details of and simulate ~10 MHz electron oscillations in the last quadrupole magnet when we flood the beam with electrons from an end wall.

Emerging measurements that show promise but are not thoroughly tested, include the trapping depth of electrons.

## INTRODUCTION

Electron clouds and gas pressure rise limit the performance of many major accelerator rings, and may limit linacs being developed as drivers for heavy-ion-inertial fusion (HIF) [1] and for high-energy-density physics (HEDP) [2]. We are working to understand the underlying physics through the coordinated application of experiment, theory, and simulation. This paper emphasizes the experimental component, accompanying papers discuss the theory and simulations [2,3].

Electron cloud effects generally occur gradually, over many passes of a beam through an accelerator ring. However, we have demonstrated in both experiment and simulation that high electron densities, approaching the beam density, can significantly degrade beam properties in the short distance of 2 lattice periods in a linac. We study these effects in the High-Current Experiment (HCX), shown in Fig. 1. HCX transports a 4 $\mu$s flattop pulse (superbunch-like) with 0.18 A of 1 MeV K+ ions. Details of the beam transport through 10 electrostatic quadrupoles, preceding the 4 magnetic quadrupoles, have been reported [4]. The beam has a space-charge potential of 2 kV, corresponding to a tune depression of 0.10 in a long lattice. This potential approaches that of HEP and other accelerator rings and is sufficient for many experiments on the generation, accumulation, effects, and mitigation of electron-cloud effects.

*Work supported by the U.S. DOE by Univ. of California, Lawrence Livermore and Lawrence Berkeley National Laboratories under contracts No. W-7405-Eng-48 and DE-AC02-05CH11231.

## DIAGNOSTICS AND ELECTRON CONTROL ELECTRODES

The HCX in the region of four magnetic quadrupoles is shown in Fig. 1. To the left is the D2 diagnostic region between 10 electrostatic quadrupoles and the 4 magnetic quadrupoles. Each magnetic quadrupole has 30 cm long magnetic field coils in a 47 cm length elliptical tube that has major and minor inner radii of 5 cm and 3 cm respectively. Between each pair of magnets, and after the last one, diagnostic access is provided in a 5 cm gap, each with 7 ports. Arrays of diagnostics are mounted on the outside of octagonal tubes that fit within the elliptical-quadrupole-magnet beam tubes. Two different arrays are placed within the third and fourth quadrupoles. A gap of about 0.7 cm annular space is provided between the octagonal diagnostics mounting tube and the elliptical magnet bore for the recessed diagnostics and cables. These diagnostics include electrodes shielded from the beam electric field by grids that we will discuss further here, recessed capacitive electrodes, and 8 cm$^2$ electrodes that are flush with the diagnostics tube in the fourth quadrupole.

A suppressor ring electrode, surrounding the beam after it exits the last quadrupole magnet, is biased to –10 kV to prevent ion-induced electron emission off an end wall (a slit plate) from reaching the magnets, or it can be left unbiased to allow electrons to be emitted from the end wall and to flow upstream into the magnets. In recent experiments, we replaced the ring electrode with a pair of parallel plates – both of these can be biased negatively to suppress electron emission similar to the ring suppressor; but they can also be biased to produce an electric dipole field across the beam. Electrons are then attracted to

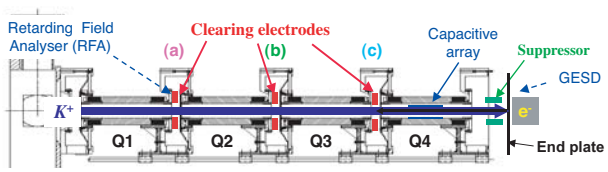


Figure 1. HCX in region of 4 quadrupole magnets, with clearing electrode rings between magnets and a suppressor electrode ring after the last magnet.

the positive plate, enabling electron emission from the end wall plus ionization of desorbed gas to be measured.

When the suppressor electrodes are biased negatively, they also prevent electrons from leaving the beam at the exit of the four quadrupole magnets. At the entrance to the magnetic quadrupoles, the exit electrode of the electrostatic quadrupoles is also negative, which prevents electrons from being lost upstream of the quadrupole magnets. These electrodes provide axial confinement and the positive-ion beam potential provides radial confinement of electrons, so that electrons are confined both axially and radially. Once trapped, we expect electrons to remain trapped until the beam potential decreases at the end of the pulse, unless removed earlier by clearing electrodes.

## NEW QUANTITATIVE MEASUREMENTS

We are using a retarding field analyzer (RFA), derived from the ANL design [5], but with the addition of a grid that serves as an ion repeller, Fig. 2 [6]. Previous experiments have used similar analyzers to measure the flux and energy of electrons reaching the wall, yielding a qualitative measurement of electron cloud density. We measure the expelled ion energy distribution, which perhaps counter-intuitively provides a more quantitative measurement of electron cloud density than does measuring electrons directly. This is because we measure low energy ions from beam impact on gas, which are expelled by the beam potential, providing a measurement of the potential, and of the degree to which it is reduced by the accumulation of electrons [7].

Electron currents to clearing electrodes provide an independent and corroborating measurement of electron accumulation as a function of time. When they are biased positively, they remove electrons that would otherwise accumulate between the negative electrodes at either end of the quadrupole magnets. Integration of this current yields the time-dependent electron line charge that would accumulate in the case when clearing electrodes are off.

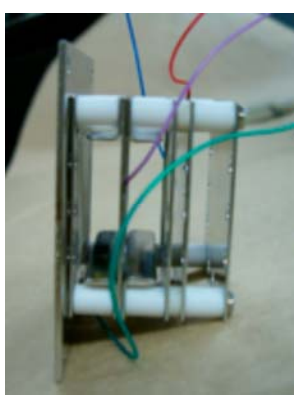

Figure. 2. Retarding field analyzer (RFA) includes ion repeller grid to enable ion as well as electron energy distribution measurements.

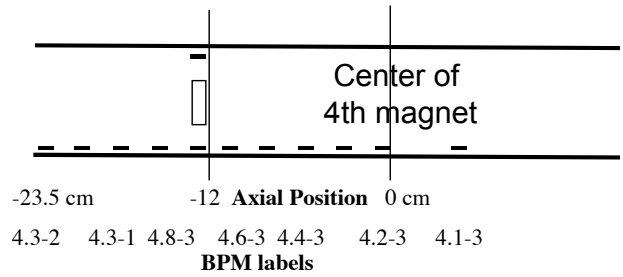


Figure 3. Array of BPMs in the fourth magnet, electrostatically coupled to the beam.

To obtain the line charge of electrons when clearing electrodes are on, we divide the clearing electrode current by the electron drift velocity in quadrupole magnets (~0.6 m/$\mu$s) [7].

We have studied the scaling of electron emission with K+ ion energy between 50 and 393 keV. due to ions impinging at angles near grazing incidence on stainless steel. We found that emission scaled with the electronic component of ion stopping in stainless steel, dE/dx, as has been found previously at higher energies [8]. However, the emission did not vary with $1/\cos(\theta)$, unlike measurements with 1 MeV K+ [9] and higher energies [10]. We have successfully modeled angle of incidence variation, with a modified dE/dx model [6].

To benchmark WARP/POSINST simulations of oscillations in electron charge that grow and propagate upstream against the beam, we have temporarily replaced the array of diagnostics mounted on an octagonal tube with an axial array of capacitively-coupled electrodes in the fourth magnetic quadrupole, Fig. 3. The measurements agree with simulations finding the same wavelength (5 cm), frequency range (5-15 MHz), and amplitude of oscillations. The amplitudes are compared by computing the rms power averaged over a range of 1-31 MHz, Fig. 4. The agreement is very good, except that the simulation shows the amplitude decreasing beyond the end of the constant quadrupole field where the magnetic field has dropped to 0.5 of the central value, whereas the

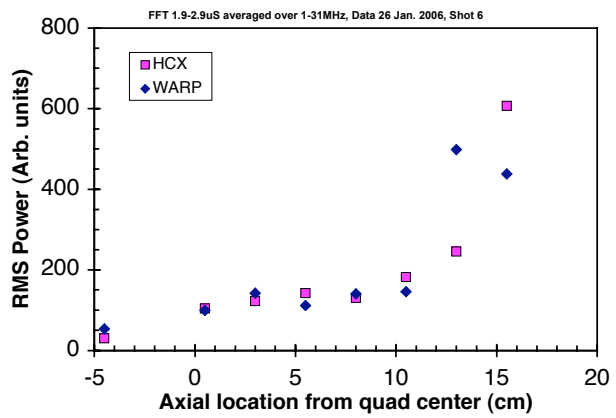


Figure 4. RMS power in electron oscillations, from BPM measurements in HCX and simulated with WARP code.

Experimentally measured amplitude doesn't decrease until the next electrode at 17.5 cm (not shown) where the magnetic field is 0.1 of the central value.

## EMERGING MEASUREMENTS

One method of measuring the accumulation of electrons at the end of a beam pulse would be to measure the current of electrons that detrap during the beam tail when the beam potential is falling to zero. To accomplish this, it is important to shield the capacitively-coupled current from the beam head and tail; because the magnitude and polarity of the integrated charge is the same at the end of a pulse for a capacitively coupled beam with no electrons as the electron charge collected from a completely neutralized beam. In addition to shielding against capacitive pickup, if the collectors are in a magnetic field, it is essential that the collectors be located where electrons can flow along field lines to it.

Therefore, gridded-electron collectors (GEC) are located at azimuths where quadrupole field lines enter the beam tube, see Fig. 5. Then, electrons that are detrapped as the beam potential falls to zero at the end of the pulse can flow along magnetic field lines from the beam to the collector. Preliminary results were discussed at PAC05 [11]. This azimuthal location forgoes the magnetic suppression that is possible at azimuths where magnetic field lines are tangent to the surface [12], but which would also render electron collection impossible. A consequence of this location is that we can bias the collector to suppress electron emission from either the collector or the grids, but not from both.

As mentioned, the purpose of the grids is to shield the GIC/GEC from capacitive pickup, which exceeds the expected current of expelled ions or detrapped electrons by 3 orders of magnitude. The effectiveness of the grids was tested before installation by pulsing square waves on a metal cylinder at the beam position, relative to the grounded diagnostics beam tube. The signal to gridded collectors was compared with the signal to bare collectors, scaled to the same area, to determine the shielding factor of the grids. Electromesh grids of 90 mesh/inch, 90% transparency, were sandwiched between the stainless steel diagnostics beam tube and a thin stainless steel frame, which was spot-welded around the periphery, grounding the grids to the diagnostics beam tube. A single grid provided a shielding factor of 30, which was inadequate compared with the expected capacitive pickup. Adding a second grid, one on the inside and one on the outside of the 0.4 mm thick beam tube, increased the shielding factor to 400-600.

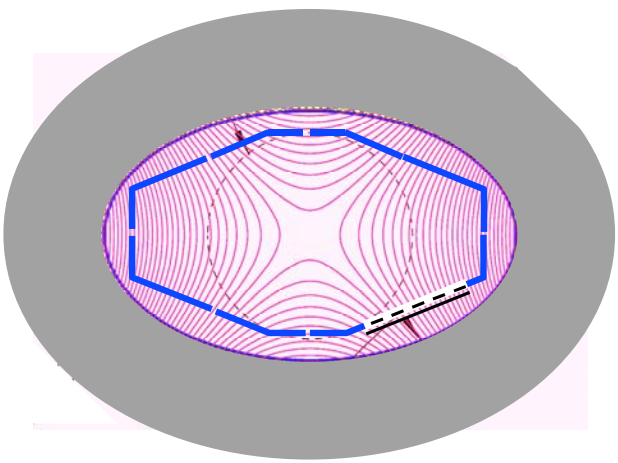

Figure 5. Gridded electron collector (GEC) is located azimuthally in quadrupole magnet so that electron which detrap can reach collector along magnetic field lines.

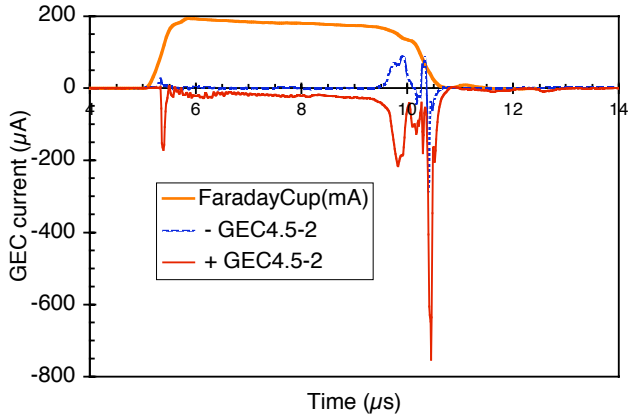


Figure 6. The currents to a gridded electron collector (GEC) are shown for negative and positive collector bias, and are compared to the time dependence of the end Faraday cup, which is time shifted to the GEC axial position. The suppressor is biased to $V_s$ = -10 kV, and the three clearing electrodes are all biased to +9 kV.

During commissioning tests [11], we found that the GEC current-voltage characteristic was flat within 10% for positive collector bias between 20 and 80 V. This is one indication that the GEC measurements are reliable, in that the current doesn't vary significantly with the collector bias.

The effects of the collector bias are compared for positive and negative bias in Fig. 6. During most of the pulse the polarity of the current reverses from collecting electrons on a positive electrode to emitting electrons

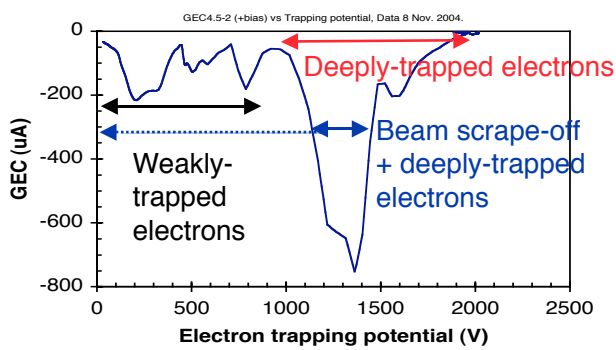


Figure 7. Current of detrapped electrons at end of pulse as a function of trapping potential.

from a negative electrode; however at two times in the beam tail, the current to a negatively biased electrode becomes negative (see the next paragraph). In Fig. 6, we also compare the Faraday cup after the magnets, time shifted to the position using capacitive pickup from the beam to the flush short collectors (FLS) at the same axial position as the GEC to calibrate the time-shift.

We plot the GEC current as a function of the electron trapping energy in Fig. 7. We obtain the trapping energy from the Faraday cup current decay at the end of the pulse as follows: The peak beam potential on axis with minimal electrons is 2000 V [7,13]. We set the point where the beam current begins a more rapid decay to zero (~9.5 $\mu$s), and the end of the current decay to 2000 V (~10.5 $\mu$s), scaling potentials in between to be proportional to the change in beam current. When we compare both polarities of GEC collector bias, we see certain periods with a negative bias that have a negative current: we believe that at those periods, extreme beam scrape off generates an electron cloud that is dense enough to overcome the negative electrode bias and give an electron current into the collector. At other times, emission from the electrode gives a positive current. The periods with negative current correspond to ~600 V and 1100 V trapping potential so we regard the GEC currents as suspect near these times.

To obtain the electron line charge, we observe that the GEC's not only collect electrons from all magnetic flux that passes through the beam but also from most of the remaining region outside the beam. Since quadrupole fields have four similar regions azimuthally, we multiply the measured signal to one of these regions by 4. Axially, the GEC aperture is 2.8 cm long, the transmission of the double grid totals 0.77, so we can obtain the line-charge per meter from the integrated electron charge to the GEC collector during the beam tail by multiplying by (4/(0.028*0.77)) = 186. Applying this factor and numerically integrating the negative tail spike, we obtain the electron line-charges $\lambda_e$, which can be normalized to the ion beam charge ($/\lambda_b$ = 0.082 $\mu$C/m), yielding $\lambda_e/\lambda_b \approx$ 0.14.

One source of electrons to the GEC is beam loss to the walls, resulting in electron emission. A possible measure

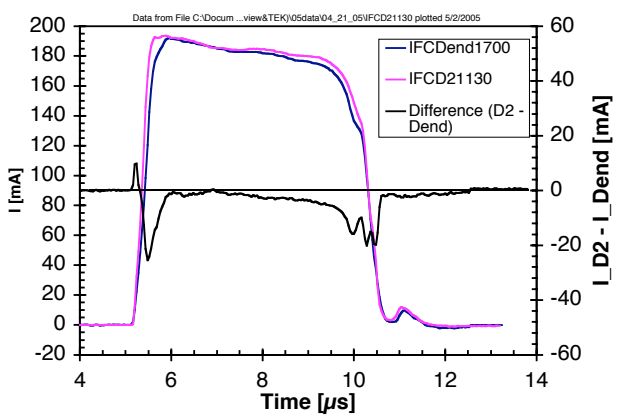


Figure 8. Faraday cup currents before the quadrupole magnets (D2), after the magnets (Dend), and the difference.charge.

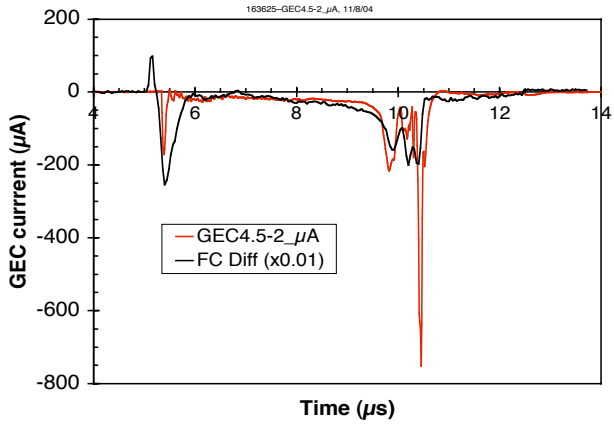


Figure 9. The difference in Faraday cup current during transport through the magnets (times 0.01) is compared with the GEC current.

of this is the difference in the beam current measured with Faraday cups before and after the four magnetic quadrupole magnets. In Fig. 8, we subtract the beam current after the magnets (FC-Dend) from that before the magnets (FC-D2). The difference, which is apparently due to halo scrape off within the magnets, bears a startling resemblance to the GEC current, see Fig. 9, where we multiply the difference in beam current by 0.01. To estimate the total electron production between the Faraday cups, we can multiply the GEC current by the ratio of the total beam length between the ESQ electrodes and the suppressor electrode (~2.4 m) times the factor listed above for electron line charge per meter length of 186, for a total factor of 445. This implies that 4.4 electrons accumulate for each ion lost, much smaller than the electron emission coefficient of ~100 near grazing incidence [9].

This similarity in waveform suggests that the GEC could be measuring electron as they are generated, rather than measuring the accumulated electrons as they detrap at the end of the pulse. If so, this would be a less valuable diagnostic, its only advantage over a flush electrode that measures electron emission and collection would be that

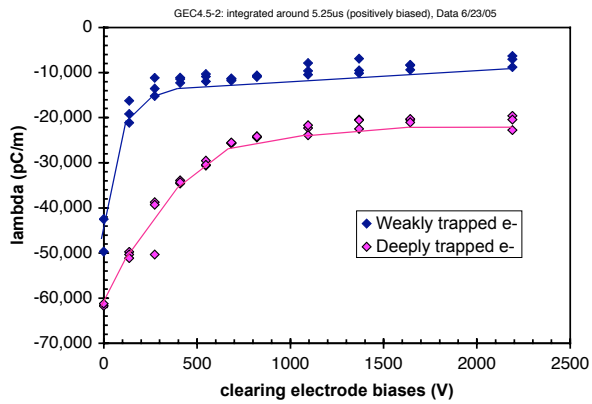


Figure 10. Weakly-trapped electrons (GEC first peak at end of pulse) are removed with lower clearing electrode bias than are deeply-trapped electrons (GEC final peak at end of pulse).

it is shielded from capacitive pickup. However, analytic estimates of axial beam spreading, due to the beam space charge, predict similar time shifts between the two Faraday cup positions to those seen in Fig.8 that may account for the head and tail spikes. WARP modeling should be able to determine how much of the results of Fig. 8 are produced by space-charge expansion of the beam.

A more positive indicator is the effect on the GEC current of varying the clearing-electrode bias for which we find that the peak that we label as weakly-trapped electrons is removed by a clearing bias of only 150-300 V, whereas removal of the peaks that we label as deeply-trapped electrons requires ≥1000 V, see Fig. 10. This is just the behavior that we would expect for accumulated electrons: weakly trapped electrons have turning points at larger radii, so require relatively low clearing bias to pull the turning points into the clearing electrodes. Deeply trapped electrons, on the other hand, have turning points at smaller radii, further from the clearing electrodes so require higher clearing bias to pull these electrons out to the clearing electrodes. If the GEC were only measuring electrons as they were produced, then both the peaks that we label as weakly and deeply trapped would consist of electron just produced at a beam tube, and both peaks would be removed with the same ease by the clearing electrodes.

To recapitulate, the final peak of the GEC current, corresponding to deeply-trapped electrons, is difficult to interpret in a quantitative manner: Beam scrape off of the tail contributes to a portion of the current measured during the detrapping of these electrons. So measurements of deeply-trapped electrons are only qualitative at present. Furthermore, electron emission cannot simultaneously be suppressed from both the collector and the grids, so some error must be expected.

The initial peak of the GEC current during the beam tail corresponds to weakly-trapped electrons. The near proportionality of the GEC current to beam losses throughout the pulse in Figs. 8 & 9 appears to be misleading, because varying the bias on the clearing electrodes affects the nominal weakly and deeply trapped electron peaks in Fig. 10 as would be expected. Therefore we conclude that the GEC waveforms provide semi-quantitative measurements of weakly trapped electron populations.

In future work, we plan to study weakly-trapped electrons, that in Fig. 7 appear to have a trapping width of ~400 eV. If these electrons originate from the beam tube, we would expect a narrower trapping width. This will complement other studies that capitalize on our new capabilities to measure absolute electron line charge as a function of time in order to measure electron accumulations from different sources, and to determine the sensitivity of the beam to varying amounts of electrons from each source.

*This work performed under the auspices of the U.S. DOE by Univ. of California, Lawrence Livermore and Lawrence Berkeley National Laboratories under contracts No. W-7405-Eng-48 and DE-AC02-05CH11231.

## REFERENCES

[1] B. G. Logan, F. M. Bieniosek, C. M. Celata, et al., "Overview of the US heavy ion fusion research," Nuclear Fusion 45, 131 (2005).
[2] H. Qin, et al., THAY05, this conference.
[3] J-L. Vay, THAW01, this Conference
[4] L. R. Prost, P. A. Seidl, F. M. Bieniosek, C. M. Celata, A. Faltens, D. Baca, E. Henestroza, J. W. Kwan, M. Leitner, W. L. Waldron, R. Cohen, A. Friedman, D. Grote, S. M. Lund, A. W. Molvik, and E. Morse, "High current transport experiment for heavy ion inertial fusion," Phys. Rev. Special Topics – Accelerators and Beams (PRSTAB) 8, 020101 (2005).
[5] R. A. Rosenberg, and K. Harkay, Nucl. Instrum. Methods A 453, 507 (2000).
[6] M. Kireeff Covo, Arthur Molvik, Alex Friedman, Glen Westenskow, John J. Barnard, Ronald Cohen, David Grote, and Steven M. Lund, Peter Seidl, Joe W. Kwan, Grant Logan, David Baca, Frank Bieniosek, Christine M. Celata, and Jean-Luc Vay, Jasmina L. Vujic, "Beam Energy Scaling of Ion-Induced Electron Yield from $K^+$ Impact on Stainless Steel," PRSTAB 9, 063201 (2006).
[7] M. Kireeff Covo, Arthur Molvik, Alex Friedman, Jean-Luc Vay, Peter Seidl, Grant Logan, David Baca, and Jasmina L. Vujic, "Absolute Measurement of electron cloud density in a positively-charged particle beam," Accepted for publication in Phys. Rev. Lett.
[8] H. Rothard, K. Kroneberger, A. Clouvas, E. Veje, P. Lorenzen, N. Keller, J. Kemmler, W. Meckbach and K.–O. Groeneveld, Phys. Rev. A 41, 2521 (1990).
[9] A. W. Molvik, et al., "Gas desorption and electron emission from 1 MeV potassium ion bombardment of stainless steel," PRSTAB 7, 093202 (2004).
[10] P. Thieberger, et al., Phys. Rev. A61, 042901 (2000).
[11] A.W. Molvik, M. Kireeff Covo, A. Friedman, R. Cohen, S.M. Lund, J.J. Barnard, LLNL; F. Bieniosek, P. Seidl, D. Baca, J.-L. Vay, C.M. Celata, W.L. Waldron, LBNL; J.L. Vujic, UC Berkeley, "Experiments Studying Desorbed Gas and Electron Clouds in Ion Accelerators," 2005 Particle Accelerator Conference, Knoxville, TN, May 16-20, 2005.
[12] A.W. Molvik, P. A. Seidl, F. M. Bieniosek, R. H. Cohen, M. Kireeff Covo, L. Prost, Nuc. Instrum,. And Methods A, 544, 194-201 (2005).
[13] S. Lund, private communication (2004).